30th AIAA Applied Aerodynamics Conference
25 - 28 June 2012, New Orleans, Louisiana

AIAA 2012-2667

A Transonic Laminar-Flow Wing Glove Flight Experiment: Overview and Design Optimization

Michael J. Belisle,[1] Matthew W. Roberts,[1] Thomas C. Williams,[1] Matthew W. Tufts,[1] Aaron A. Tucker,[2]
William S. Saric,[3] and Helen L. Reed[4]
Texas A&M University, College Station, Texas, 77843-3141

The Subsonic Aircraft Roughness Glove Experiment (SARGE) is a hybrid natural laminar flow and passive laminar flow control flight test that will be carried out under the auspices of the NASA Environmentally Responsible Aviation initiative. The primary goals of the SARGE experiment are to 1) achieve natural laminar flow to 0.60 chord on the suction side at up to 22 million chord Reynolds number and 2) at conditions of at least 22 million chord Reynolds number, demonstrate the effectiveness of a passive array of discrete roughness elements in extending laminar flow beyond the natural transition location. The test will be conducted on a test article having 35° leading-edge sweep at 0.75 Mach and lift coefficient of at least 0.5. In cooperation with NASA Dryden Flight Research Center, Texas A&M has completed the optimized aerodynamic design of the wing glove, as well as flight test and instrumentation planning.

Nomenclature

AoA	= Angle of attack for infinite swept wing, rotated about axis parallel to leading edge
c	= Chord length
CF	= Crossflow
C_l	= Section lift coefficient normalized by local chord
C_p	= Pressure coefficient
f	= Disturbance frequency (dimensional)
H	= Altitude
M	= Mach number
N	= Smith–Van-Ingen N-factor
r	= Leading-edge radius
Re_c	= Chord Reynolds number
Re_θ	= Attachment-line momentum thickness Reynolds number
Re'	= Unit Reynolds number
U_∞	= Freestream velocity
t/c	= Airfoil thickness ratio
TS	= Tollmien-Schlichting
x/c	= Chord length ratio
$(x/c)_{tr}$	= Predicted chord length ratio for onset of laminar–turbulent transition
α	= Local glove angle of attack
β	= Local glove angle of sideslip
ε	= Leading-edge thickness ratio
Λ_{LE}	= Leading edge sweep angle

[1] Graduate Student, Department of Aerospace Engineering, Member AIAA
[2] Graduate Student, Air Force Institute of Technology Civilian Institution Program, Senior Member AIAA
[3] Distinguished Professor, Department of Aerospace Engineering, AIAA Fellow
[4] Professor, Department of Aerospace Engineering, AIAA Fellow

λ = Crossflow wavelength parallel to leading edge (dimensional)
λ_1 = Target crossflow wavelength parallel to leading edge (dimensional)
λ_2 = Control crossflow wavelength parallel to leading edge (dimensional)
ν = Freestream viscosity

I. Introduction

Swept-wing laminar flow control (SWLFC) on transport aircraft has long been an area of active academic and commercial research interest. Mature SWLFC could result in drag and fuel savings of as much as 10%. In comparison with other technologies, SWLFC would be the single largest contributor to near-term efficiencies on transport aircraft (Collier, 2010). In order to realize SWLFC on production aircraft, additional technology maturation is needed.

The NASA Environmentally Responsible Aviation (ERA) initiative is a national plan for maturation of near and medium term improvements in transport aircraft fleet fuel efficiency, emissions, and noise. The Subsonic Aircraft Roughness Glove Experiment (SARGE) is one such initiative intended to raise the Technical Readiness Level (TRL) of passive SWLFC using a spanwise-period array of micron-sized Discrete Roughness Elements (DREs).

Saric, Carrillo, & Reibert (1998) demonstrated that passive laminar-turbulent transition delay is possible using a judiciously designed pressure distribution in conjunction with DREs placed near the attachment line on a swept wing. At chord Reynolds number Re_c = 2.4 million (unit Reynolds number Re' =0.4 million/ft) on a swept wing with leading edge sweep Λ_{LE} = 45°, results in the Klebanoff–Saric Wind Tunnel showed that, as long as transition is due to stationary crossflow, DREs have the capability to delay transition past the pressure minimum. The Flight Research Laboratory at Texas A&M University has completed a successful in-flight demonstration of DREs on a Λ_{LE} = 30° swept wing at Re_c = 8 million and Re' = 1.7 million/ft (Carpenter, Saric, & Reed 2010; Saric, Carpenter, & Reed 2011; Rhodes, Reed, Saric, & Carpenter 2010). Roughness receptivity studies are presently in progress under these conditions in order to quantify the role of roughness amplitude in generating crossflow waves. In addition, this technique has been demonstrated for supersonic flight (Saric, Reed, & Banks 2004). The overall goal of SARGE is execute a successful flight test that extends the demonstrated effectiveness of DREs to a transport-relevant Mach number, Re_c, and C_l in addition to Re' as demonstrated previously.

Belisle, Neale, Reed, & Saric (2010) demonstrated the feasibility of a laminar-flow glove experiment at Re_c = 15–20 million using a Gulfstream II as host aircraft. The logical extension of these efforts is to design a single experiment capable of covering this range as well as extending the test to higher Re_c in the 22–30 million range. Demonstrating section lift coefficient (C_l) and Re' representative of transport aircraft is an additional requirement. The preliminary design of an experiment under these conditions was presented in Belisle, Roberts, Tufts, Tucker, Williams, Saric, & Reed (2011). This paper presents the final, optimized iteration of the design using the outer-mold line (OML) optimization method of Hartshorn, Belisle, and Reed (2012). A companion paper presents detailed analysis of the design using viscous, full-aircraft flowfield calculations and linear stability results (Roberts, Reed, & Saric 2012).

II. Flight experiment concept and overview

For freestream Mach numbers greater than about 0.3, it is not possible to replicate the flight environment in a ground-based wind tunnel. Turbulence in the flight environment is essentially large scale; the smaller turbulence scales that affect boundary-layer transition are absent. This has a marked effect on the mechanism for transition on a swept wing. In a typical wind tunnel, with relatively high turbulence intensities, transition is typically dominated by travelling crossflow (Deyhle & Bippes, 1996). In flight, however, transition is dominated by stationary crossflow, which is the primary transition mechanism influenced by DRE technology.

A. DRE Rationale

Passive control of transition using DREs in flight is the logical solution after considering the other options for LFC on transport aircraft. The first option is suction, which has a robust history of successful flight and wind tunnel demonstrations (Braslow, 1999; Joslin, 1994). However, the complexity and reliability of the suction system is a concern, and thus suction has not to date been adopted on a large scale on production aircraft.

The second option is to unsweep the wings. In this case, transition would be due solely to the Tollmien-Schlichting (TS) instability, as attachment line contamination and crossflow (CF) instability would be eliminated. Then, TS could be controlled using a sufficiently favorable pressure gradient. This is a solution that has been employed to some degree on low-speed aircraft, as well as on control surfaces and nacelles of aircraft like the Boeing 787. However, for the wings as whole on high subsonic transport aircraft, the wave-drag penalty would be significant and likely outweigh any gain from application of laminar flow.

The third option is to polish the leading edge to a surface roughness in the vicinity of 0.3 micron RMS. CF, unlike TS, is a three-dimensional instability that is highly sensitive to surface roughness and free-stream turbulence levels, rather than irrotational disturbances like sound. The unknown relationship between surface roughness height and initial amplitude of CF disturbances is a major focus of current receptivity research. Even so, a highly polished leading edge has been empirically shown in flight to allow transition due to stationary crossflow to occur at *N*-factors (using linear stability theory, LST) as high as $N = 14$, in contrast to a more operationally relevant leading edge (surface roughness circa 1–2 micron RMS), where transition can be expected to occur at $N = 9$. The sensitivity of crossflow to surface roughness is one of the primary complicating factors in applying the e^N method for transition prediction in swept-wing LFC (Arnal, Casalis & Houdeville 2008). Despite the performance of a polished leading edge in this respect, operational concerns and maintenance are seen as significant downsides.

Therefore, with active control, unswept wings, and polished leading edge eliminated, passive control using DREs represents a promising option.

B. Experimental requirements

The primary experimental requirements are set forth by ERA and are summarized briefly as follows. In the range of $Re_c = 15$–22 million, natural laminar flow shall be demonstrated (i.e., without the use of DREs). The ability of DREs to repeatedly delay transition by 50% shall be demonstrated for $Re_c \geq 22$ million. (i.e., if natural transition is at $x/c = 0.40$, DREs shall delay transition to at least $x/c = 0.60$. For all conditions, the unit Reynolds number $Re' \geq 1.4$ million/ft. Finally, other parameters shall be representative of transport aircraft: leading edge sweep $\Lambda_{LE} \geq 30°$, section lift coefficient $C_l \geq 0.5$, and Mach number $M \geq 0.72$.

C. Host aircraft configuration

Following an aircraft search in Belisle et al. (2010), the Gulfstream III (G-III), manufactured by Gulfstream Aircraft Corporation from approximately 1980 to 1986, was selected as the most suitable platform to host this flight test. The G-III is a business jet with maximum operating $M = 0.85$, service ceiling $H = 45000$ ft, and a wingspan of 23.7 m (77 ft 10 in). Full specifications of the aircraft are shown in Table 1.

With the glove mounted on the aircraft, the flight envelope is modified as shown by the blue box in Figure 1. Re_c is controlled by varying altitude. Angle of attack (AoA) is controlled through low-bank angle turns that effectively increase the weight of the aircraft, necessary since cruise AoA is dependent on a variety of factors including altitude and fuel loading. The primary test points, described below in Section II.F, are at $M = 0.75$.

Table 1. G-III specifications.

Parameter	Value
Wing Span	23.72 m (77 ft 10 in)
Overall Length	25.32 m (83 ft 1 in)
Overall Height	7.43 m (24 ft 4½ in)
Gross Wing Area	86.83 m^2 (934.6 ft^2)
Wing Leading Edge Sweep	31.7°
Maximum Takeoff Weight	31,615 kg (69,000 lb)
Long-Range Cruising Speed	Mach 0.77
Maximum Cruising Speed	Mach 0.85
Maximum Operating Altitude	13,720 m (45,000 ft)

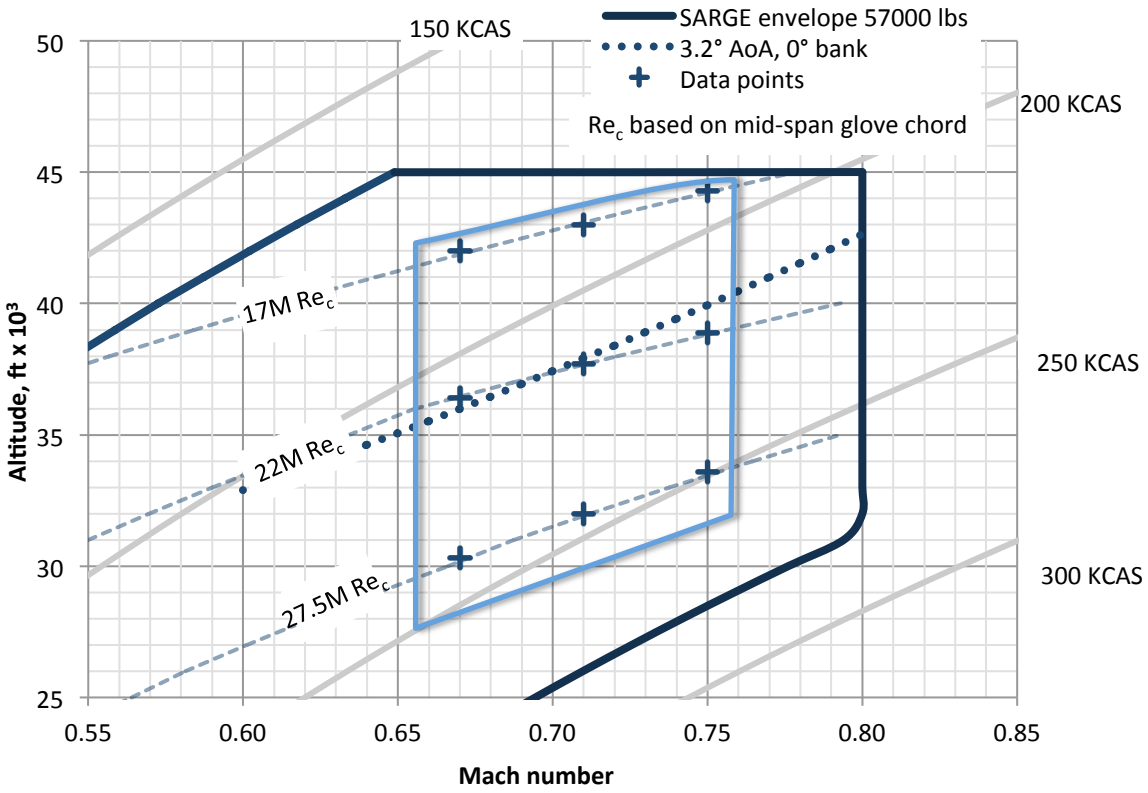

Figure 1. Science objective flight envelope, assuming c = 14.5 ft midspan chord.

D. Wing glove configuration

The concept selected for this flight test is an instrumented wing glove, shown in planform view in Figure 2 and rendered in Figure 3, below. The glove will be attached to the port wing of the testbed G-III. The glove consists of

several components. The main test section is 6 feet in span, extending from buttock line (BL, measured in inches from the fuselage centerline) BL198 to BL270. This placement was guided by the engine effect study of Belisle et al. (2010). The glove is located sufficiently outboard of the engine pressure field where the engine effects are accountable and inboard of the aileron so as to not adversely affect aircraft control. The main test section is divided into an interchangeable leading edge section for $x/c < 0.15$, the main body section from $0.15 < x/c < 0.62$, and the aft fairing into the host wing surface at the rear spar (forward of the control surfaces and spoilers). On the pressure side, the glove is blended into the host wing surface at $x/c = 0.32$ and designed such that the G-III wing provides a portion of the test surface (Section III.B). Inboard and outboard of the test section are fairings that facilitate the development of spanwise uniform flow over the test section. As described in Section III.B, the entire glove surface is optimized as a single surface with the focus on matching the test section pressure distributions. Since the glove extends forward of the host aircraft leading edge, the inboard fairing also acts as a Gaster bump (i.e. stagnation point) that prevents the propagation of attachment line disturbances from the G-III wing (after Gaster 1967). Continuous surface curvature is maintained at all interfaces in order to avoid undesirable disturbance sources arising from discontinuities in curvature.

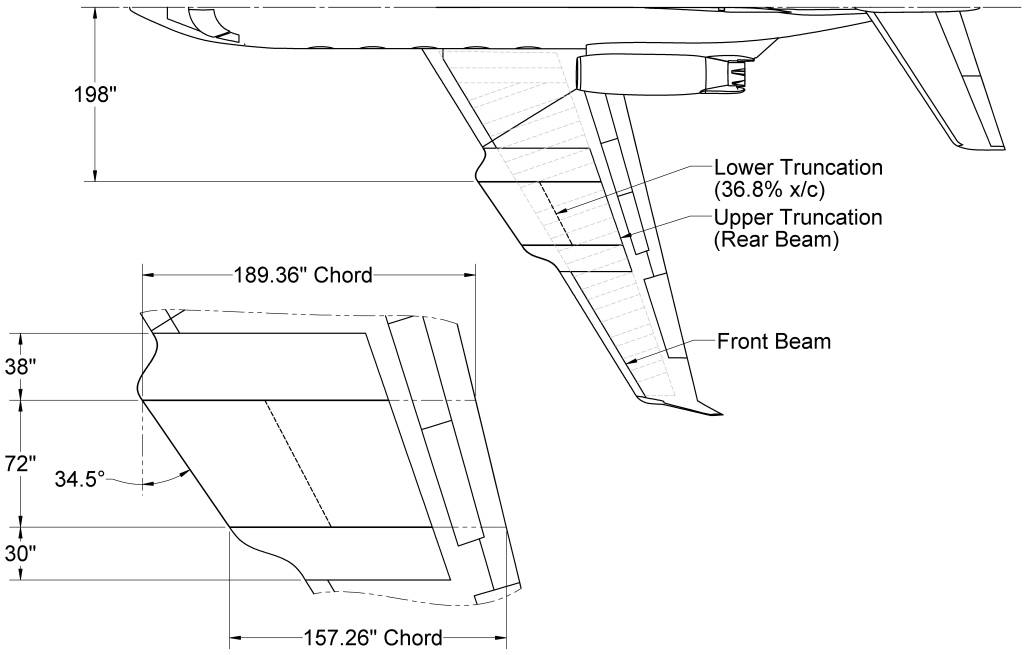

Figure 2. Planform layout of the wing glove

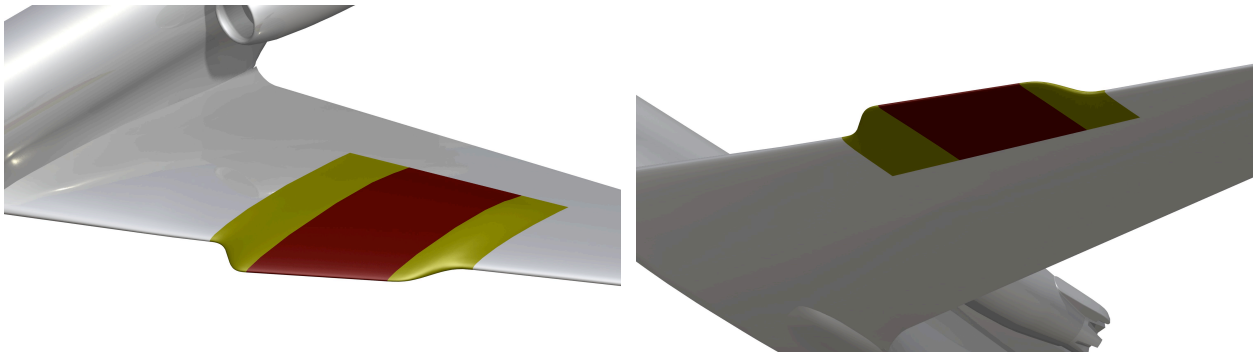

Figure 3. Rendering of wing glove on G-III port wing.

The width of the test section, diagrammed in Figure 4, was chosen to provide enough surface area to facilitate at least the minimally required 14-in spanwise section of laminar flow. The figure shows the test section shaded between the empirical "domain-of-influence" lines that are assumed to exist due to the finite span of the glove. The lines are distorted by the inviscid streamlines and the boundary conditions on the fairing, resulting in an inboard-directed skew. There is approximately a 40-in usable span at x/c = 0.6, more than sufficient to meet the 14-in requirement outlined in the SARGE project requirements.

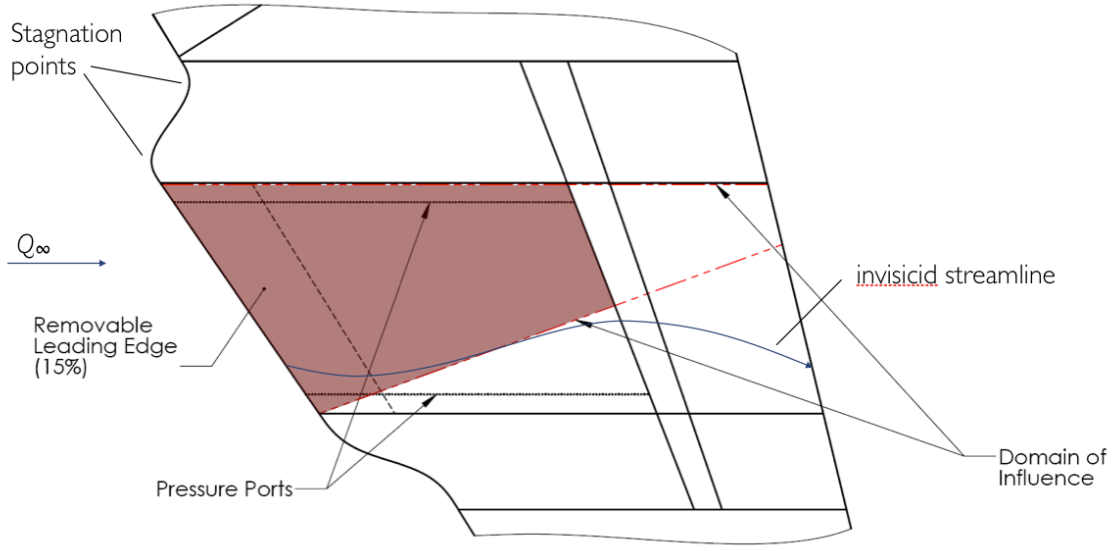

Figure 4. Layout of test section between assumed 10° domain of influence lines.

E. Glove construction and tolerances

The glove is designed as a floated wing glove having composite construction. The floated design requires 2-in OML-OML clearance over the glove test section on the suction side, which is included as a constraint in the optimization process. The intent behind a floated construction, as opposed to bonding the glove directly to the wing, is to isolate the glove from the host wing and to avoid undesirable deformation that led to cracks in a prior glove study (Meyer, Trujillo & Bartlett 1987).

Three leading edges will be constructed: two polished (0.3 micron RMS) leading edges, one with pressure ports and one without; and a operationally relevant, painted surface finish (1–2 micron RMS) without pressure ports. Since the pressure ports on the leading edge can generate undesirable turbulent wedges, the full suite of pressure measurements will be made during the initial phase of calibration flights.

F. Flight experiment description

A detailed description of the flight-test plan and instrumentation suite is covered in Belisle et al. (2011), summarized briefly here. The flight test plan consists of two phases. Phase 1 is an initial set of flights to acquire glove pressure distributions and define the in-flight AoA band for laminar flow, which may be different than the computational data band due to wing deformation that cannot be robustly quantified without accurate in-flight measurements of the wing deformation.

The second phase of flights comprises the principal research flights and is separated into two parts: the NLF flights are in Part 2A. These flights establish the success of the secondary NLF objective (no DREs, Re_c = 15–22 million) on both the polished and operationally relevant leading edges (without pressure ports). NLF flights will also be conducted at Re_c corresponding to the DRE test conditions, as a NLF baseline is needed at the DRE conditions in order to quantify the extent of laminar flow achieved.

The main part of the research program, the DRE test flights, is conducted in Phase 2B. This phase is about three-quarters of the flight hours allocated to the experiment. The DRE flights will utilize both the polished and operational leading edges to demonstrate the effectiveness of DREs under multiple levels of surface roughness. The DRE flights will be conducted using appliqué elements, although follow-on experiments may consider plasma actuators or microbubble techniques for control. Multiple heights, spacings, and shapes of appliqué DREs will be considered.

The primary laminar-flow diagnostic is IR thermography, which has been used successfully in previous flight experiments (Carpenter et al. 2010). IR thermography relies on the difference in adiabatic recovery temperatures between laminar and turbulent flow to identify transition, which is approximately 1°C at M = 0.75. The entire instrumentation suite is listed in Table 2 and diagrammed for the suction side in Figure 5. Surface-mounted thermocouples will measure surface temperature to obtain the proper boundary conditions for TS instability calculations (for which higher wall temperature has a destabilizing effect). Surface-mounted hot-film arrays will be used to acquire frequency spectra and used as a secondary diagnostic (on the suction side) to determine transition location. On the pressure side, there is no visual access for IR thermography, so hotfilms and thermocouples will be the primary diagnostic.

Table 2. Wing glove specifications.

Sensor	Purpose
IR Camera	Visualize boundary-layer transition on glove
Pressure ports	Measure pressure distribution on glove, enable calculation of lift coefficient
5-hole probe	Obtain flow angles and velocities near glove
Kulites	Measure freestream static and total pressure fluctuations
Thermocouples	Monitor glove surface temperatures
Hotfilms	Measure boundary layer frequency spectra in order to verify transition location
Strain gauges	Measure stress on glove
High frequency accelerometers	Monitor dynamic response of glove and wing structure
Standard camera	Wing deflection measurements

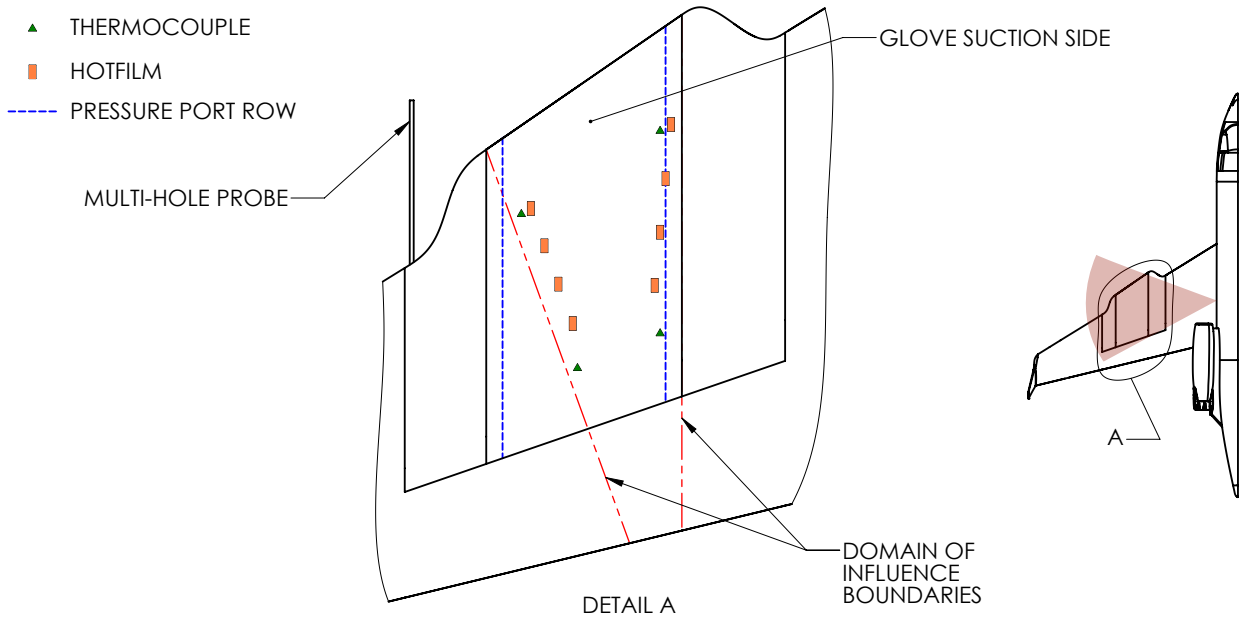

Figure 5. Suction-side instrumentation layout.

Other critically important instrumentation includes pressure ports for C_p measurements (where stripatubing will be considered on the pressure side since the G-III has a wet wing that does not facilitate subsurface pressure taps), a high-resolution camera to quantify wing deformation (using a technique following Burner, Lokos & Barrows 2005), Kulites for measurement of freestream pressure and temperature fluctuations, and a 5-hole probe for local flowfield conditions. The output from the 5-hole probe will be provided to the pilots in the form of a cockpit display so that the pilots are flying directly to the relevant test conditions.

The typical flight maneuver used to stabilize on the design AoA is a level turn at small bank angle (less than about 30°). The angle of bank is chosen to slightly increase the aircraft load factor that in turn increases the glove AoA to the design AoA. The design AoA is typically greater than the aircraft cruise AoA and as fuel is burned for a given flight condition the angle of bank also increases to maintain a particular glove AoA. Pilots use the research cockpit display to maintain test conditions (Mach number, Reynolds number, glove AoA, glove sweep angle) using power, aileron, and rudder inputs. Elevator inputs are required only to maintain an approximately level flight path to maintain stable glove AoA within tight tolerances. Onboard research crew monitor instrumentation to monitor data quality and communicate a successful test point completion with the flight crew and coordinate efficient progression of points within the science envelope.

III. Glove design

Although the philosophies for NLF and DRE SWLFC design are similar, there are a few important differences that need to be balanced in a hybrid design such as SARGE. The prevailing design philosophy in SWLFC design is to mitigate streamwise and attachment-line instabilities and concentrate on meanflow modifications to reduce the growth of CF waves. The methodology is summarized here; complete details may be found in Belisle et al. (2011).

A. DRE Design Philosophy

The first prerequisite in SWLFC is to contain streamwise and attachment line instabilities. The C_p is designed such that the streamwise stability N-factors (log of the amplitude ratio) do not become too large according to the familiar e^N method (for an overview, see for example Arnal & Casalis 2000). Therefore, an airfoil conducive to LFC by DREs features a uniformly accelerated flow so that TS waves are controlled to maintain the N-factors well below $N \approx 6$. With wing sweep, making the pressure gradient more favorable will excite crossflow instability, and therefore a balance must found between controlling TS and destabilizing CF.

Attachment-line instabilities are controlled following a method suggested by Pfenninger (1977) and Poll (1985). A constraint on the leading-edge radius r requires that Re_θ, the attachment-line momentum thickness Reynolds number, be less than 100:

$$Re_\theta = 0.404\sqrt{\frac{Q_\infty r_{LE}\sin^2\Lambda_{LE}}{\nu(1+\varepsilon)\cos\Lambda_{LE}}} < 100$$

For simplicity, the leading-edge thickness ratio, ε, is taken to be zero (i.e., the worst case).

Stabilizing TS instability naturally encourages crossflow growth. In the flight environment, the quiescent freestream environment ensures that stationary crossflow is the dominant instability. One first identifies the most unstable stationary crossflow wavelength that is expected to cause transition, λ_1. For convenience, crossflow wavelengths are measured parallel to the leading edge. Linear stability theory accurately predicts this target wavelength and the neutral point at which it first becomes unstable. Then one studies stationary crossflow of shorter wavelengths, λ_2, as candidate for the control wavelengths that the DREs will excite. The observation is that the C_p distribution can be so designed such that these control waves, which are about half the wavelength of the most-unstable wave, will grow sufficiently and then decay, thus changing the basic state and preventing the most-unstable wave from dominating. The overall effect is that transition is delayed. The SARGE C_p is designed such that crossflow waves are excited in the DRE regime ($Re_c \geq 22$ million) to allow demonstration of DRE control, but stable enough at lower Re_c so that NLF is sufficient to achieve laminar flow to $x/c = 0.60$.

An additional consideration in the crossflow instability is the sensitivity to surface roughness. Unlike the streamwise instability, which is largely insensitive to surface roughness, crossflow instability is highly sensitive to roughness. Thus, the quality of finish of the SARGE glove in the leading edge region (approximately $x/c \leq 0.10$) is an important parameter in this experiment. The experiment will consider two surface finishes: a smooth, polished leading edge and a painted or "operational" leading edge similar to a transport aircraft. From Carpenter et al. (2010), the polished surface can sustain crossflow N-factors as high as 14, while the painted leading edge will transition around $N = 9$.

B. Design methodology

The optimized design of the glove follows from the insights discussed in Belisle et al. (2011) and Hartshorn et al. (2012). In Belisle et al. (2011), a glove design (TAMU-05-04) was presented that consisted of a straight loft between two defined airfoil sections. Although this design marginally achieved the desired pressure gradient in the mid-span section, the inboard and outboard pressure distributions were not well suited to laminar flow. Hartshorn et al. (2012) describes the optimization method employed for this design in detail.

The first step in the optimization is to develop the target pressure distribution. One of the defined pressured distributions from TAMU-05-04 was used as a starting point, with additional attention given to stabilizing TS based on the results discussed in Malik, Liao, Lee-Rausch, Li, Choudhari, & Chang (2011). First, the curve was parameterized using B-Spline curves. Then by assuming an infinite swept wing, the C_p was perturbed and boundary-layer stability calculations were performed without updating the physical geometry in each iteration. This approach is valid as the direct boundary-layer solution method employed by the boundary layer solver, WINGBL2 (Pruett, 1994), does not account for curvature and the changes in geometry are "small." LST calculations were performed in LASTRAC (Chang 2003) using the boundary solution from WINGBL2. The range of unstable frequencies and wavelengths calculated was typically found to be within 1 kHz $\leq f \leq$ 10 kHz for a TS wave normal to the leading edge (i.e., zero spanwise wavenumber) and 1 mm $\leq \lambda \leq$ 40 mm for stationary CF ($f = 0$). The WINGBL2/LASTRAC calculations were verified against the Q3BL/LST3D code (Malik 1997) and found to be in good agreement. The optimized target pressure distribution is shown in Figure 6.

These stability results predict that the pressure distribution will achieve the project requirements. The pressure distribution achieves the target section $C_l = 0.5$ at the design $M = 0.75$. A representative calculation of LST N-factors in Figure 7 shows that the NLF requirements are nominally achieved by the target C_p distribution, with transition expected to occur at $x/c = 0.52$ for a highly polished leading edge, triggered by the most-unstable wavelength of 10 mm. Streamwise instability in the leading-edge-normal direction was calculated to be negligible on the suction side.

For DRE control at $Re_c = 22$ million, shown by the LST N-factors in Figure 8, transition is expected at approximately $x/c = 0.4$ for a highly polished leading edge. DREs with spanwise spacing of 4 mm are a viable candidate for control to stabilize the most unstable wavelength of 8–9 mm. DREs can be expected to delay transition

back to at least x/c = 0.60 in this case. At Re_c = 30 million, expected transition moves forward to x/c = 0.32 and 3 mm is a candidate control wavelength.

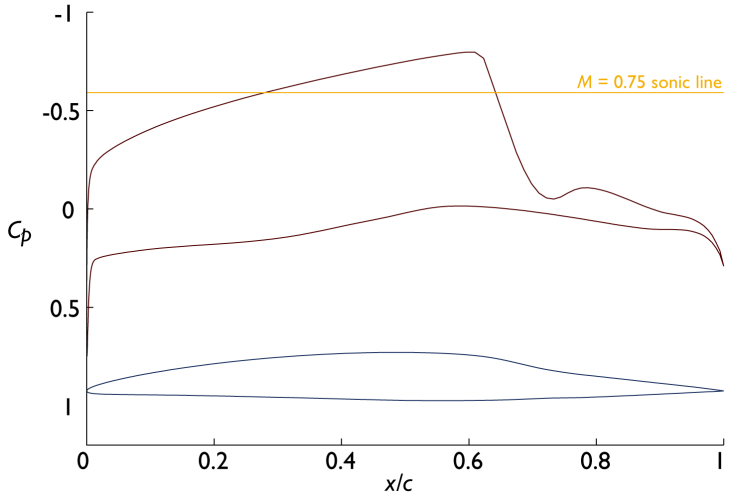

Figure 6. Target pressure distribution for glove optimization.

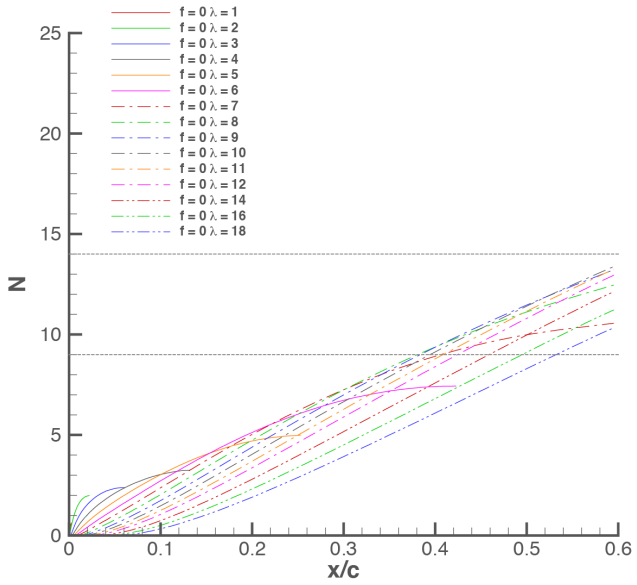

Figure 7. Target C_p LST N-Factors in NLF regime, M = 0.75, Re_c = 15.0 million (referenced to BL270, c = 4.0 m, H = 44800 ft). Dashed horizontal lines show expected transition N-factors for polished (N_{tr} = 14) and operational (N_{tr} = 9) leading edge roughness. Spanwise wavelengths are in mm.

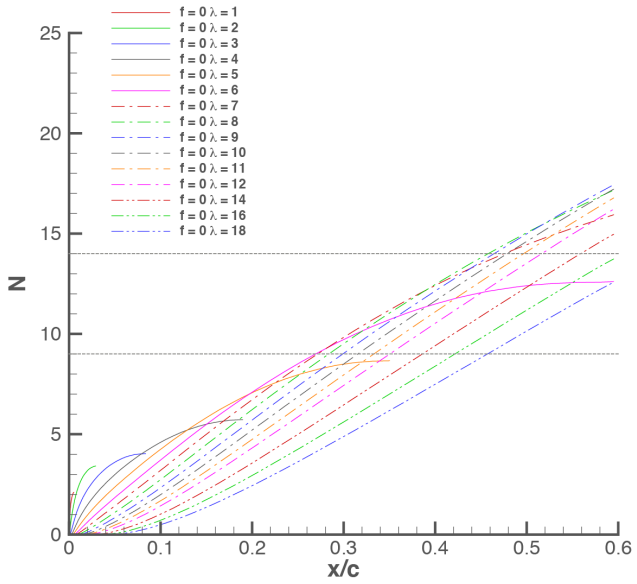

Figure 8. Target C_p LST N-Factors in DRE regime, $M = 0.75$, $Re_c = 22$ million (referenced to BL234, $c = 4.4$ m, $H = 38300$ ft). Dashed horizontal lines show expected transition N-factors for polished ($N_{tr} = 14$) and operational ($N_{tr} = 9$) leading edge roughness. Spanwise wavelengths are in mm.

With the target pressure distribution determined, the next step in is to optimize the glove shape to achieve relatively spanwise-uniform flow over the extent of the glove test section. The method uses TRANAIR (Boeing, 2009) along with custom perturbation and objective function routines. TRANAIR is a full-potential code with a coupled integral boundary-layer model. C_p distributions as calculated using TRANAIR compare favorably with Navier-Stokes solutions, and thus are suitable for stability analysis in the design phase. The C_p distribution along a constant span section (principally BL234, the midspan of the glove) from TRANAIR is passed to WINGBL2 to obtain a boundary-layer solution that is then analyzed using LASTRAC. The stability results are compared to those from the target distribution.

C. Design results and initial stability analysis

The resulting design from this optimization process is given the appellation TAMU-06-05. The stability results presented here are analyzed during the design process. Detailed computational assessment of the optimized glove is presented in the companion paper Roberts et al. (2012). Inboard (BL198), Center (BL234), and Outboard (BL270) airfoil sections are shown in Figure 9. Figure 10 is a comparison of the TAMU-05-04 (unoptimized) and TAMU-06-05 (optimized) pressure distributions at these span locations. As can be seen, the optimized pressure distributions much more closely follow the target distribution, especially when considering the slope of the C_p, an important consideration for stability analysis. Further refinement of the target C_p may allow the spanwise uniformity to be improved.

Figure 11 shows a comparison of LST N-factors at BL234 with the target-C_p N-factors from Figure 8. The optimized results show that the LST N-factors compare favorably with the target-C_p N-factors. Even though the optimized C_p profiles are offset from the target C_p, the important feature to note is that the C_p slope is matched consistently across the glove span. This feature leads to similar stability characteristics across the entire span of the glove. An assessment showing LPSE results is shown in Figure 12. Stationary crossflow stabilization due to curvature does not appear to be a concern in the final optimized glove design, as compared with the unoptimized design (cf. Malik et al. 2011, Figure 14).

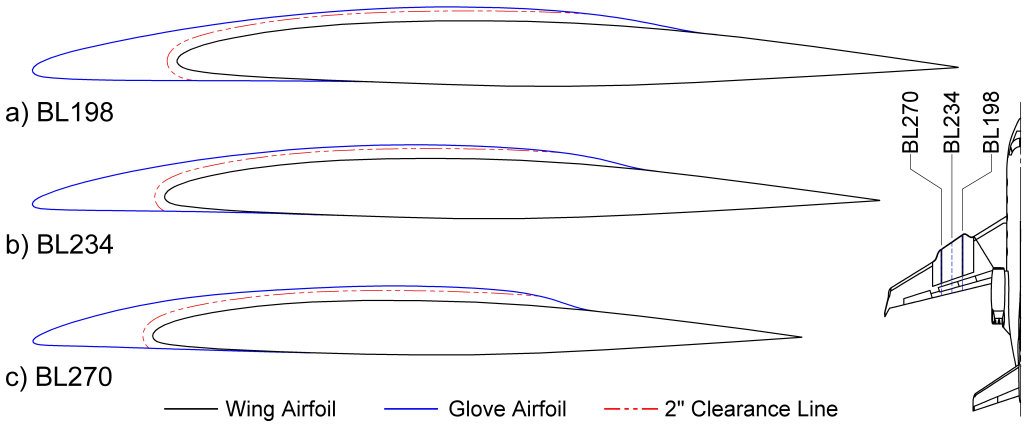

Figure 9. Wing glove airfoil sections at a) BL198, b) BL234, and c) BL270.

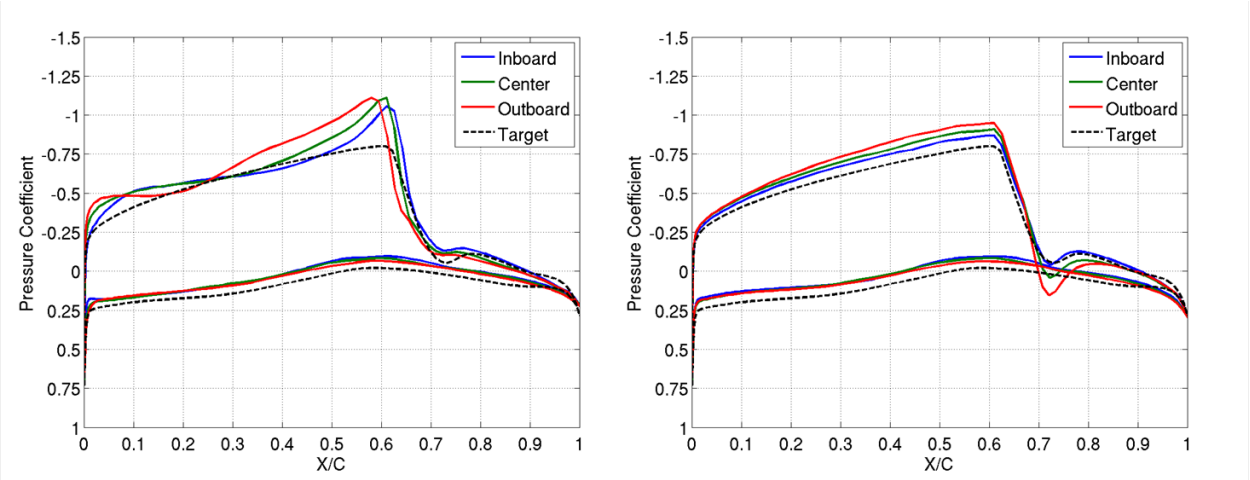

Figure 10. TAMU-05-04 (unoptimized, left) and TAMU-06-05 (optimized, right) pressure distributions.

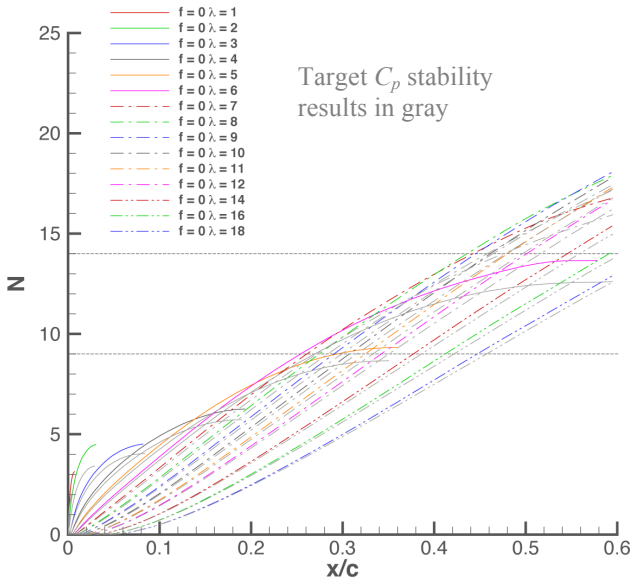

Figure 11. Optimized glove section (BL234) LST N-Factors in DRE regime, $M = 0.75$, $Re_c = 22$ million ($c = 4.4$ m, $H = 38760$ ft). Dashed horizontal lines show expected transition N-factors for polished ($N_{tr} = 14$) and operational ($N_{tr} = 9$) leading edge roughness. Spanwise wavelengths are in mm. Grey lines show LST results for Target C_p (Figure 8).

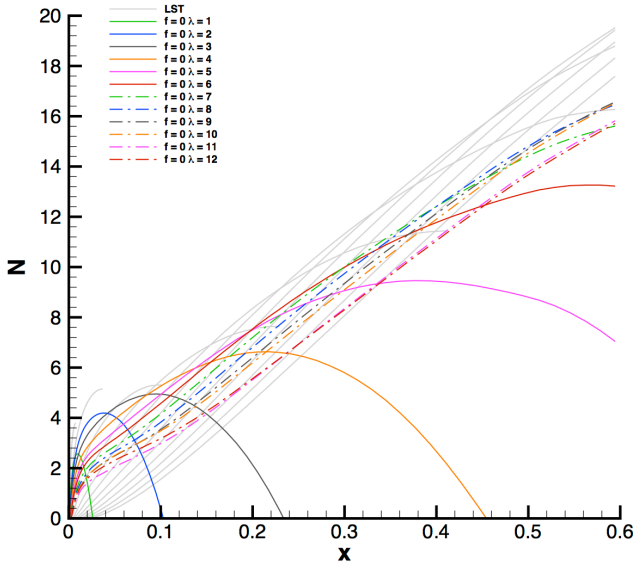

Figure 12. Optimized glove section (BL234) LPSE N-Factors in DRE regime, $M = 0.75$, $Re_c = 22$ million ($c = 4.4$ m, $H = 36730$ ft). Spanwise wavelengths are in mm. Grey lines show glove LST results for same conditions (Figure 11).

IV. Conclusions

A laminar-flow wing glove design, flight experiment, instrumentation planning, and design stability results for in-flight demonstration of SWLFC using passive DREs has been presented. The OML of the design has been successfully optimized, with the focus on improving the spanwise uniformity over the unoptimized design. The design is predicted to meet the objectives of the SARGE project towards raising the TRL of DRE technology for future application to transport aircraft. The design has been selected to proceed to Preliminary Design Review.

Acknowledgments

This work was supported under ViGYAN subrecipient grant C10-00350, ATK grant SP00029509, and AFOSR grant A4760.

This work is a cooperative effort with NASA Dryden Flight Research Center and NASA Langley Research Center. Technical interactions with the NASA Centers are gratefully acknowledged. In particular, Fletcher Hartshorn is thanked for his work in developing the optimization method.

References

[1] Arnal D, Casalis G. 2000 Laminar-turbulent prediction in three-dimensional flows. *Progress in Aerospace Sciences*. 36(2):173–91

[2] Arnal, D., Casalis, G. & Houdeville, R. 2008 Practical transition prediction methods: Subsonic and transonic flows. In *Advances in Laminar-Turbulent Transition Modelling, NATO RTO-EN-AVT-151*, pp. 7-1–7-34.

[3] Arnal D, Vermeersch O. 2011 Compressibility effects on laminar–turbulent boundary layer transition. *International Journal of Engineering Systems Modeling and Simulation* 3(1): 26–35.

[4] Belisle MJ, Neale TP, Reed HL, Saric WS. 2009 Design of a Swept-Wing Laminar Flow Control Flight Experiment for Transonic Aircraft. *AIAA-2010-4381*

[5] The Boeing Company. 2009 TRANAIR User's Manual.

[6] Braslow, Albert L. 1999 A history of suction-type laminar-flow control with emphasis on flight research. *NASA Monographs in Aerospace History* 13.

[7] Carpenter AL, Saric WS, Reed HL. 2010 Roughness Receptivity in Swept-Wing Boundary Layers—Experiments. *Int'l J. Eng. Sys. Modeling and Simulation,* 2(1):128-38

[8] Chang C-L. 2003 The Langley stability and transition analysis code (LASTRAC): LST, linear & nonlinear PSE for 2-D, axisymmetric, and infinite swept wing boundary layers. *AIAA-2003-0974*

[9] Chang C-L, Choudhari M. 2005 Boundary-layer receptivity and integrated transition prediction. *AIAA-2005-0526*

[10] Collier, Jr., F. S. 2010 Overview of NASA's Environmentally Responsible Aviation (ERA) project. Invited presentation at the 48th AIAA Aerospace Sciences Meeting. Orlando, Florida.

[11] Deyhle, H., Bippes, H. 1996 Disturbance growth in an unstable three-dimensional boundary layer and its dependence on environmental conditions. Journal of Fluid Mechanics 316, 73–113.

[12] Gaster, M. 1967 On the flow along swept leading edges. *Aero. Q.* **18**, 165–184.

[13] Joslin, R. D. 1998 Overview of laminar flow control. *NASA TP-1998- 208705*.

[14] Malik M. 1997 Boundary-layer transition prediction toolkit. *AIAA-1997-1904*.

[15] Meyer, Robert R., Trujillo, Bianca M. & Bartlett, Dennis W. 1987 F-14 VSTFE and results of the cleanup flight test program. In *Research in Natural Laminar Flow and Laminar-Flow Control,* pt. 3, pp. 819–844. NASA.

[16] Hartshorn F, Belisle MJ, Reed HL. 2012 Computational Optimization of a Natural Laminar Flow Experimental Wing Glove. To be presented at 50th AIAA Aerospace Sciences Meeting, Nashville, Tennessee.

[17] Malik M, Liao W, Lee-Rausch E, Li F, Choudhari M, Chang C-L. 2011 Computational Analysis of the G-III Laminar Flow Glove. *AIAA-2011-3525*.

[18] Pruett CD. 1994 A spectrally accurate boundary-layer code for infinite swept wings. NASA Contractor Report 195014

[19] Pfenninger W. 1997 Laminar flow control—Laminarization. *AGARD Report No. 654*

[20] Poll DIA. 1985 Some observations of the transition process on the windward face of a long yawed cylinder. *J. Fluid Mech.* 150:329-56

[21] Rizzetta D, Visbal M, Reed HL, Saric WS. 2010 Direct numerical simulation of discrete roughness on a swept wing leading edge. *AIAA J.* 48(11):2660–73

[22] Rhodes RG, Reed HL, Saric WS, Carpenter AL. 2010 Roughness Receptivity in Swept-Wing Boundary Layers—Computations. *Int'l J. Eng. Sys. Modeling and Simulation*. 2(1):139–48

[23] Saric WS, Carrillo RB, Reibert MS. 1998 Leading-edge roughness as a transition control mechanism. *AIAA-1998-0781*

[24] Saric WS, Carpenter AL, Reed HL. 2011 Passive control of transition in three-dimensional boundary layers, with emphasis on discrete roughness elements. *Phil. Trans. R. Soc. A* 369:1352–64
[25] Saric WS, Reed HL, Banks DW. 2004 Flight testing of laminar flow control in high-speed boundary layers. *NATO-RTO-MP-AVT-111*, Prague, Oct.